ELSEVIER

Polymer 40 (1999) 3469–3478

polymer

Temperature dependence of crystal structure of uniaxially-oriented polyethylene analysed by an X-ray imaging plate system

Kohji Tashiro[a,*], Kiyotaka Ishino[a], Toshihiko Ohta[b]

[a]*Department of Macromolecular Science, Graduate School of Science, Osaka University, Toyonaka, Osaka 560-0043, Japan*
[b]*Faculty of Life Science, Osaka City University, Sumiyoshi, Osaka 558, Japan*

Received 27 March 1998; received in revised form 17 June 1998; accepted 15 July 1998

Abstract

Crystal structure of uniaxially oriented polyethylene has been analysed as a function of temperature by using an X-ray imaging plate system equipped with software useful for the structure analysis of polymer crystals. The cell parameters *a* and *b*, the anisotropic temperature factors of the carbon atom, and the setting angle of the planar–zigzag chain measured from the *b* axis, etc., were found to show a deflection point around + 10°C. The structure and thermal motion below this characteristic point could be interpreted in terms of harmonic vibration. But, above this deflection point, the thermal motion became more remarkable, requiring an introduction of an idea of anharmonic vibration. The temperature dependence of these structural parameters is different between the samples used in the measurement. The sample oriented at relatively low draw ratio showed larger temperature dependence and a clearer deflection point around 10°C, compared with the case of the ultradrawn sample. This difference may reflect a difference in the remnant strain in the samples.

Keywords: Polyethylene; Structure analysis; Temperature

1. Introduction

In a series of papers [1–3] we clarified the usefulness of an imaging plate (IP) detector for collecting the quantitatively accurate X-ray reflection data necessary in the structural study of polymer crystals. The IP detector is highly sensitive and highly quantitative, showing a good linearity of intensity between incident and collected photons in the wide range from 1 to 10^6 photons [4]. This detector is useful also for collecting the 2-dimensional reflection pattern, allowing us to check the total image of the fiber diagram. The fiber diagram taken by the IP system can be saved as digital data onto a computer disk. Then we developed new software to analyze the reflection data and could obtain the highly-quantitatively integrated intensity of reflections after carrying out the separation of overlapped reflections reasonably [3]. Besides, the fiber diagrams were taken by using the Mo–Kα line as an X-ray source, giving a larger number of reflections than the case of the Cu–Kα line of longer wavelength. By using the thus evaluated great number of X-ray reflectional data, we could employ the so-called direct method to get the initial structure necessary for the least-squares refinement of molecular and crystal structures of polymers such as orthorhombic polyethylene, trigonal polyoxymethylene and isotactic polybutene-1 form I [3].

These characteristic features of the IP system in polymer structural analysis may drive us to perform a more refined study on the structural change of polymer crystals subjected to the various external conditions such as temperature, pressure, tension, electric field, etc. In particular, the effect of temperature on the structural parameters is considered to be quite important because the thermally-induced structural change is intimately related with the temperature dependence of the physical properties of polymer crystals. These data are important also for the investigation of thermal motions of polymer chains in the crystal regions.

In this paper an orthorhombic polyethylene (PE) was chosen as a good candidate for the above-mentioned purpose. This is because PE has a simple structure, making it possible to grasp accurately the small changes in the crystal structure. Another reason is that many reports trying to clarify the structural change of PE crystal have been published so far [5–16] mainly by means of the X-ray diffraction technique. But the results described in these papers are not consistent with each other and so the exact thermal behavior of PE crystal has not yet been definitely established. Some of these studies are now reviewed briefly below.

* Corresponding author.

0032-3861/99/$ - see front matter
PII: S0032-3861(98)00553-9

Swan [7] measured the temperature dependence of the unit cell dimensions for the unoriented PE samples, clarifying that the linear thermal expansion coefficient along the *a* axis is larger than that of the *b* axis in the temperature range of − 196 to 130°C. One of the most important crystal structure parameters of PE is a setting angle of the planar–zigzag chain, which is defined as an angle between the skeletal zigzag plane and the *b*–*c* plane. Kawaguchi et al. [12] reported that the setting angle is almost constant (ca. 45°) below 0°C but changes slightly above 0°C. They carried out the structure analysis by trial-and-error method under the constraining condition of fixed bond lengths and angles, using the 28 *hk0* reflections measured for the polyethylene single crystal. Kavesh and Schultz [10] reported that the setting angle (ϕ) becomes larger as the temperature increases from room temperature ($\phi = 45°$ at 20°C and 50° at 100°C). They analyzed the crystal structure by using only nine X-ray Bragg reflections collected for the unoriented sample, where the five structural parameters (scale factor, fractional coordinates and anisotropic temperature factors of the carbon atom) were varied to minimize the difference between the calculated and observed reflectional intensities. Iohara et al. [11] reported the temperature dependence of the mean-squared displacement parameters of the carbon atoms in the temperature range of −160 to 120°C based on the X-ray reflection data. They described also the temperature dependence of the setting angle: it does not change below 0°C ($\phi = 42°$) but increases above 0°C slightly so that the zigzag plane of the chains tends to be parallel to the *a* axis ($\phi = 44.6°$ at 60°C and 44.0° at 93°C). In their analytical work, they refined the seven parameters including the scale factor, fractional coordinates and anisotropic displacement parameters (U_{aa}, U_{bb}, U_{cc}, U_{ab}) of the carbon atoms by using the 32 reflections collected by a Geiger–Müller counter. Chatani, Tadokoro et al. [13,14] reported that the setting angle becomes larger for the sample with larger lattice strain, where the analysis was made at room temperature for the samples prepared under the various different conditions.

In this way the structural analysis of PE crystal subjected to the various conditions were reported by many authors. But, the structural parameters reported by them cannot be assumed to be determined to the highest degree of accuracy, judging from the quality and number of the observed reflectional data. As reported in the previous paper [3], we could collect the total number 45–50 of reflections for the uniaxially-oriented PE samples, much larger than the number described in the other papers [5–16], allowing us to determine the structural parameters more accurately than ever. In this paper, therefore, we will try again to clarify the details of the structural changes of PE crystal at the various temperatures by using the X-ray reflectional data evaluated by the IP system.

2. Experimental section

2.1. Samples

Two different types of PE samples were investigated. One was a linear high density polyethylene (HDPE) with $M_w = 1.26 \times 10^5$, $M_n = 2.4 \times 10^4$, and $M_w/M_n = 5.3$. Uniaxially oriented specimens of HDPE were prepared by stretching the melt-quenched sample about 15 times the original length at 110°C. The other type of PE sample was an ultra-drawn polyethylene, which was obtained from ultra-high-molecular-weight PE ($M_w = 2 \times 10^6$, HIZEX 240 M) by gel-press method [17] with the total draw ratio about 150. The Young's modulus was 160 GPa and the tensile strength was 3.5 GPa.

2.2. X-ray measurement

The X-ray diffraction data were collected by using an imaging plate system DIP1000 (MAC Science, Ltd., Japan). The X-ray generator was a SRA-MXHF (MAC Science Co., Ltd.) with graphite-monochromatized

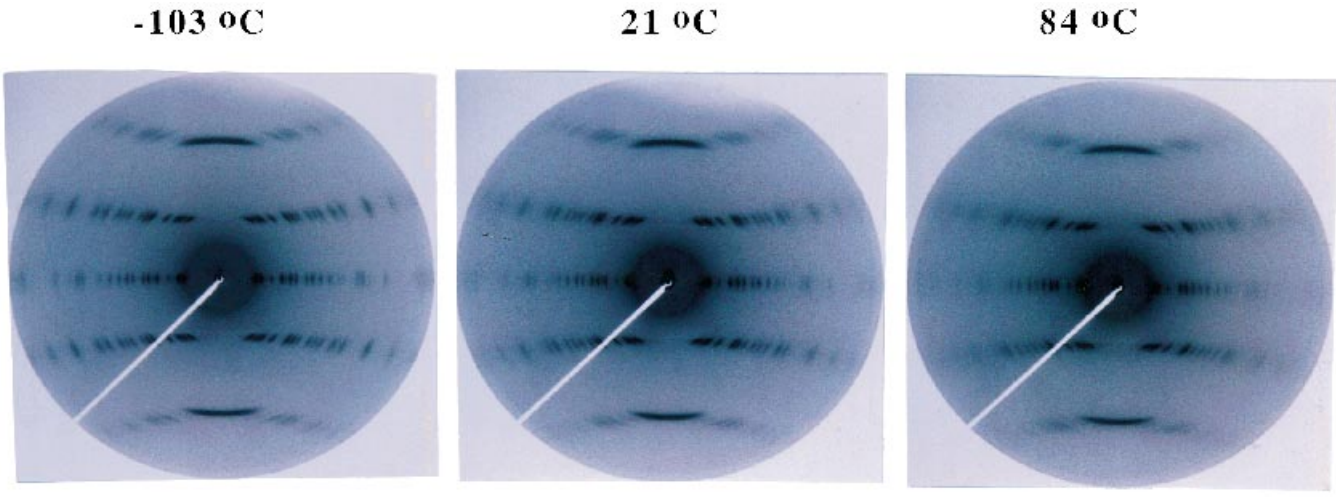

Fig. 1. X-ray fiber diagrams of uniaxially-oriented polyethylene (draw ratio 15) taken at various temperatures by the imaging plate.

Mo–Kα radiation ($\lambda = 0.71073$ Å). Measurements were carried out in the temperature range from -103 to 93°C using a Cryostream cooler with liquid nitrogen as a coolant (Oxford Cryosystem, Ltd.), where the nitrogen gas was blown to the sample directly. Temperature was monitored by a thermocouple attached directly to the sample. The temperature fluctuation was about ± 0.5°C. The sample-to-IP distance (98.9 mm) was calibrated by a silicon powder as standard sample. The measurement limit of the scattering angle 2θ was 50°.

3. Results and discussion

3.1. Brief description of the flow of structure analysis

The crystal structure of PE at each temperature was determined in the following way on the basis of our newly developed software. The details were already described in our previous paper [3].

3.1.1. Measurement and correction

The X-ray fiber diagram measured for a uniaxially-oriented sample by using a DIP1000 flat camera was transformed from the Cartesian coordinate system (x and y) to the cylindrical coordinate system (ξ and ζ). Fig. 1 shows the fiber diagrams taken at the various temperatures for the 15-times drawn PE sample. In the cylindrical coordinate system the ζ axis is defined to be coincident with the chain axis and ξ is the radius from the origin to the point in the plane projected along the chain axis. This transformation is useful for the evaluation of reflection positions on the layer lines, because the layer lines are curved in the fiber diagram taken on the flat camera but can be changed to horizontal lines in the (ξ, ζ) coordinate system. Furthermore the intensity of the whole pattern is corrected for the Lorentz factor (L) and the polarization factor (p) (Lp correction).

3.1.2. Indexing

The observed reflections are indexed by a trial-and-error method. The principle is to investigate the reciprocal lattice points satisfying the observed d-spacings. More concretely speaking, a set of circles of various radii ξ is drawn on the a^*–b^* reciprocal lattice plane of a constant ζ value and the lattice points crossing the drawn circles are searched. The lattice sizes of a^* and b^* and the angle between these two axes are changed by trial-and-error so that all the observed curves cross any lattice points once at least. This process can be made by utilizing a computer graphic technique, as reproduced in Fig. 2. This process of indexing is repeated for all the layer lines. If all the observed reflections can be indexed reasonably and consistently based on the common reciprocal lattice parameters, then it may be said that we successfully determine the unit cell parameters (a, b, c, α, β, and γ). In order to get more exact lattice parameters, the least squares calculation is made by using the data of exact peak positions of reflections which are reasonably separated by the curve fittings, as described in the following stage (Section 3.1.3).

3.1.3. Integrated intensity

The background correction and the separation of the

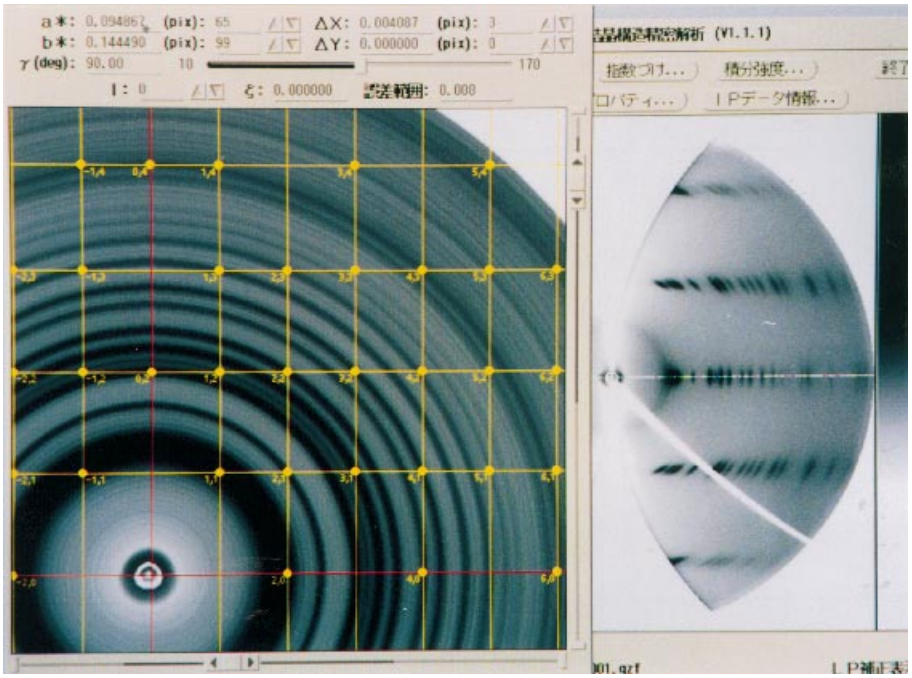

Fig. 2. Computer screen displaying the indexing process of the reflections on the equatorial line indicated by a horizontal line in the right-side diagram. The small solid circles represent the reciprocal lattice points crossed by the circles of constant ξ values.

overlapped reflections are the most important process in the flow of X-ray data analysis. Fig. 3 shows our method. A range of fiber diagram to be analyzed is zoomed up on the screen [Fig. 3(a)]. One horizontal line (and one vertical line) is drawn on an arbitrarily chosen point, and then the reflectional profile along this horizontal line (and along the vertical line) is exhibited on another screen [Fig. 3(b)]. The background of this profile is erased and the thus corrected reflectional profile is separated into components by carrying out the curve fitting, where the reflectional profile is assumed to be a combination of Gaussian and Lorentzian functions. The result of the curve separation is shown in Fig. 3(b). In this way we can know the exact peak position and the integrated intensity of each component on the line of constant ζ. This process of background correction and curve separation is repeated for the whole screen of Fig. 3(a). The group of open circles shown in Fig. 3(c) are the thus determined peak positions. The larger circle means the peak with higher intensity. By summing up the integrated intensities obtained for all the ζ lines of a particular reflection component, the total integrated intensity or the total volume of intensity can be evaluated for the individual reflection. Integration can be made automatically when the circles belonging to the particular reflection [Fig. 3(d)] are enclosed by a fan-like square. The thus analyzed reflections are indicated by red color to indicate the completion of data treatment.

The equivalent reflections in the four regions of the IP photograph should ideally have the same integrated intensity. The degree of this equivalency is represented by using the so-called R_{merge} defined by the following equation:

$$R_{\text{merge}} = \Sigma_i[\Sigma'(I_{\text{obs},i} - < I_{\text{obs},i} >)^2/\Sigma' I^2_{\text{obs},i}]/N \quad (1)$$

where $I_{\text{obs},i}$ is the observed ith-intensity and $\langle I_{\text{obs},i} \rangle$ is the averaged intensity between the equivalent four reflections. The summation Σ' is over the equivalent four reflections. The final R_{merge} is averaged for all the reflections of the total number N. In the present case of PE, the R_{merge} calculated for the collected 50–60 reflections was 2.4–5.1%, comparable to the values observed for the single crystals of low-molecular-weight organic compounds, indicating a highly quantitative data treatment in the present study.

3.1.4. Structure analysis

The structural analysis has a purpose to obtain the

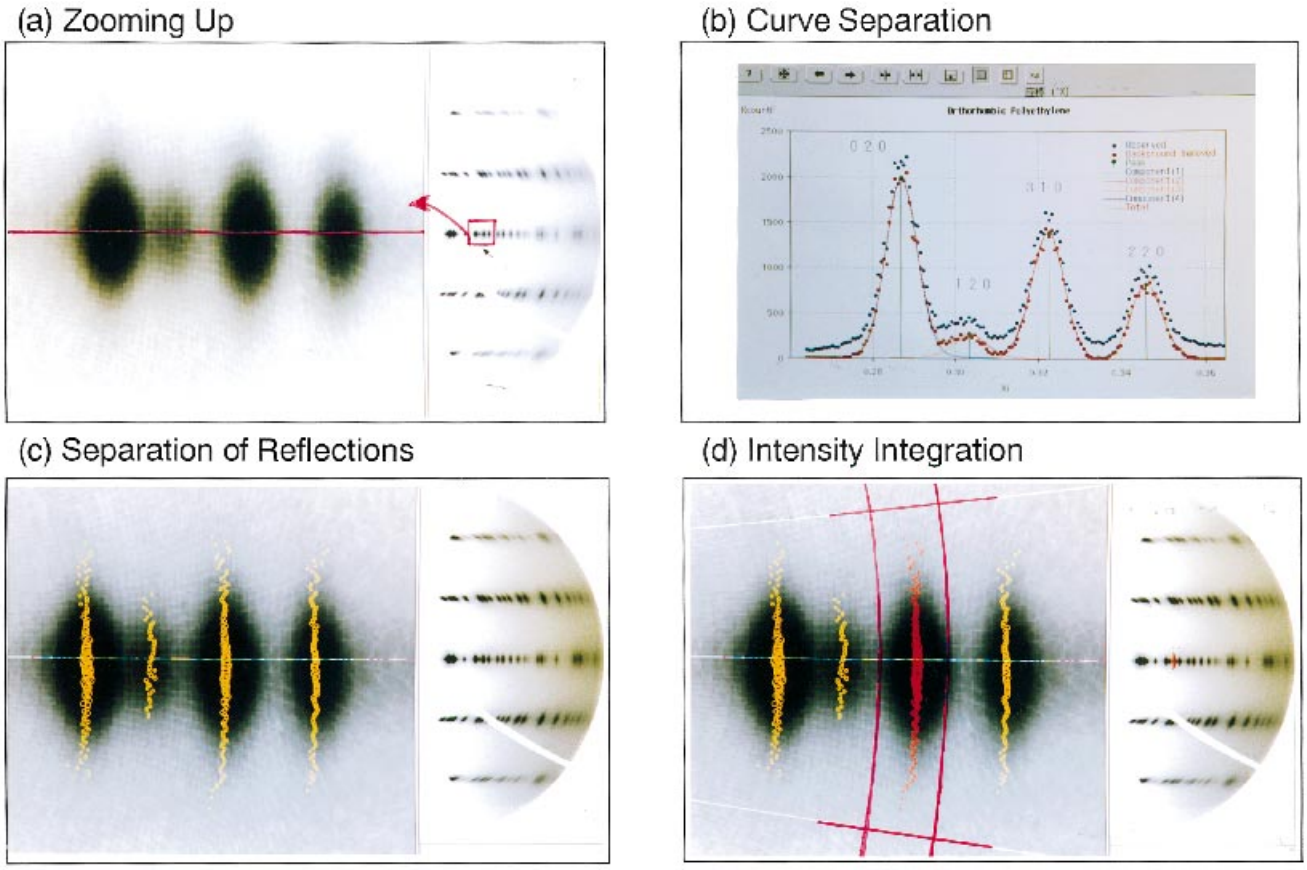

Fig. 3. (a) Zoomed-up screen of a region shown by a rectangular zone in the left-side X-ray diffraction diagram of PE; (b) Curve separation of the reflection profile shown by the horizontal line in the zoomed-up screen of (a); (c) The peak positions of the separated reflection components made for all the horizontal lines in the zoomed-up screen of (a); (d) The integration of the intensities evaluated for all the profiles belonging to a particular reflection component separated in (c).

electron density distribution $\rho(x, y, z)$ at the position (x, y, z) in the unit cell as expressed by the following equation:

$$\rho(x, y, z) = \sum_h \sum_k \sum_l F(hkl)\exp[-2\pi i(hx + ky + lz)] \quad (2)$$

where the structure factor $F(hkl)$ has a form of

$$F(hkl) \equiv \sum_x \sum_y \sum_z f(hkl)\exp[2\pi i(hx + ky + lz)]$$
$$= |F(hkl)|\exp[i\varphi(hkl)]. \quad (3)$$

In this equation $f(hkl)$ is the atomic scattering factor, $|F(hkl)|$ is the absolute value of F and $\varphi(hkl)$ is the phase angle. Based on the equation concerning the integrated intensity

$$I = ALp|F|^2 \exp[-(h^2B_{11} + k^2B_{22} + ...)]$$

(A = X-ray absorption coefficient of the sample, B_{ij} = anisotropic temperature factor, and λ = X-ray wavelength), we can know the absolute value $|F(hkl)|$. If the angles $\varphi(hkl)$ can be clarified, therefore, the electron density map $\rho(x, y, z)$ or the crystal structure can be obtained from Eq. (2). The 'direct method' is one of the most powerful techniques to estimate the phase angles on the basis of statistical treatment of the reflectional data (see, for example, [18]) and has been applied almost always to the structural analysis of single crystals of the low-molecular-weight compounds. As described in the previous paper [3], we applied this direct method to the X-ray data of synthetic polymers and succeeded in getting a reasonable set of phase angles, from which the reasonable initial structure could be obtained. This technique was applied to the present case of PE crystal measured at the various temperatures. The used software was ShelXS. In Fig. 4 are shown the positions of carbon and hydrogen atoms obtained by the direct method.

The thus determined initial structure was refined by a full-matrix least squares method. The parameters to be refined were the fractional coordinates (x_i, y_i) and anisotropic displacement parameters (U_{aa}, U_{bb}, U_{cc}, and U_{ab}) of carbon atoms, the isotropic displacement parameters of the hydrogen atoms and the scale factor. Final crystal structures of the ultra-drawn PE and 15-times drawn PE samples were determined by utilizing, respectively, 53–58 and 48–58 reflections in total. The total number of the reflectional indices taken into account in the analysis were 70–80, where the several indices (h, k, l) contribute accidentally to one reflection in some cases. The R factors were 5.3–7.6% and 8.2–12.4%, respectively, for these two samples, where the R factor is defined as:

$$R = 100 \times \Sigma_i(|F_o|_i - |F_c|_i)/\Sigma|F_o|_i(\%)$$

and $|F_o|$ and $|F_c|$ are the observed and calculated structure factors, respectively.

3.2. Structure analysis of PE as a function of temperature

Fig. 1 shows the fiber diagrams of the 15-times drawn

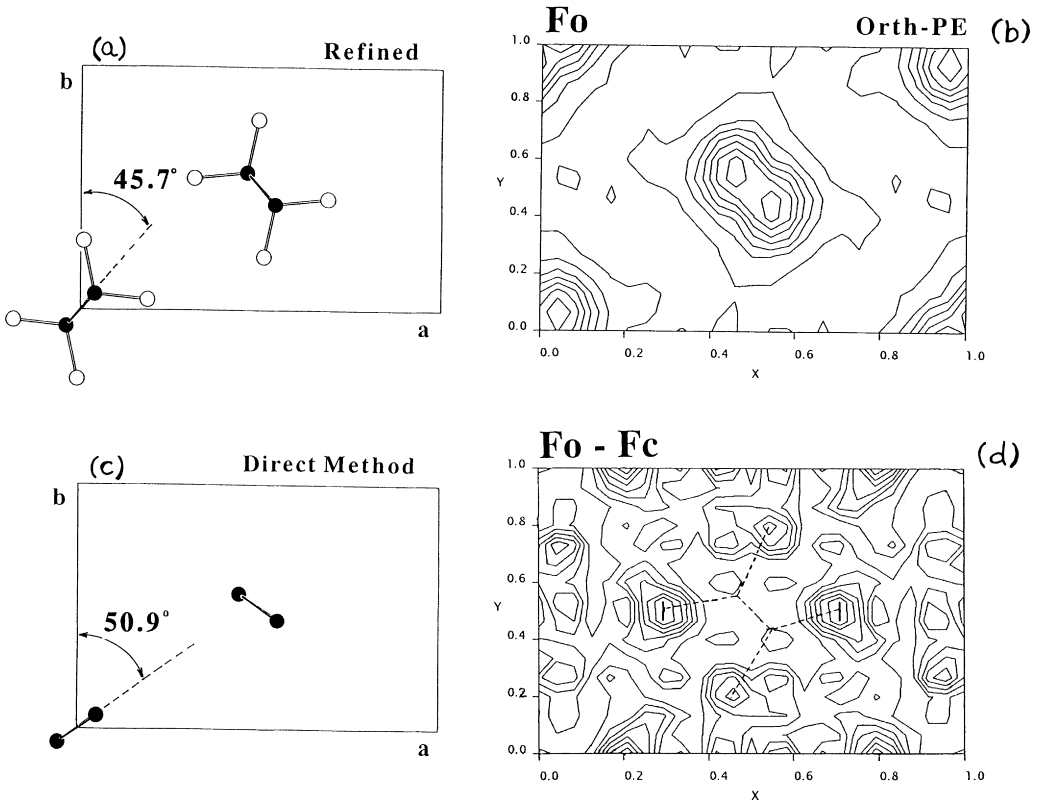

Fig. 4. (a) Crystal structure of PE obtained by refining the initial structure (c) obtained by the direct method; (b) and (d) Contour maps showing the positions of (b) carbon and (d) hydrogen atoms extracted by the direct method.

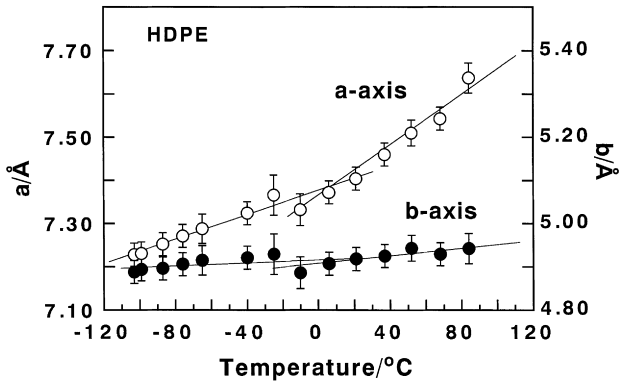

Fig. 5. Temperature dependence of the lattice parameters *a* and *b* of orthorhombic PE obtained for the normally-drawn HDPE sample.

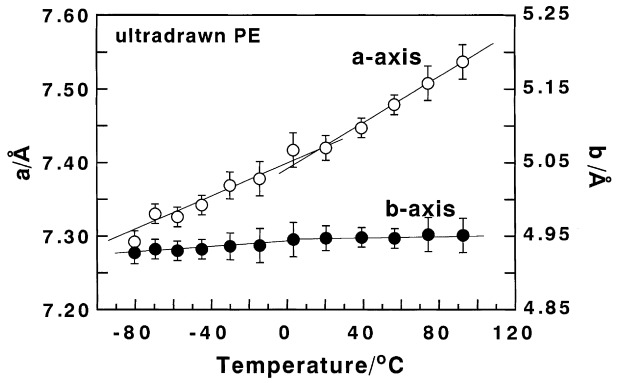

Fig. 6. Temperature dependence of the lattice parameters *a* and *b* of orthorhombic PE obtained for the ultradrawn sample.

HDPE sample taken at the various temperatures. As typically seen for the reflections at higher scattering angles (or the reflections far from the center of the photograph), the Bragg reflectional intensities became weaker at higher temperature. This may reflect the increase of thermal motion or the increase of the temperature factor at higher temperature. Table 1 shows the full set of the crystallographic data analysed for HDPE sample at room temperature, as an example. The temperature dependence of the structural parameters will be discussed in the following subsections.

3.2.1. Unit cell parameters

The temperature dependencies of the unit cell dimensions *a* and *b* for HDPE and ultra-drawn PE samples are shown in Figs. 5 and 6, respectively. It should be noted here that the unit cell parameters shown are the averaged values among those obtained for the data collected at the several independently-made measurements. The error bars indicated in these figures are the standard deviations evaluated from these data analyses. In the analysis of the data, we at first evaluated the peak positions (ξ, ζ) of the individual reflections obtained after the curve separations described in the previous subsection, and tried to estimate the unit cell parameters of *a*, *b* and *c* under the assumption of the orthorhombic unit cell. But the thus obtained cell parameters were rather dispersive and the systematic temperature dependence could not be obtained. This may come from the difficulty of the exact estimation of the peak positions of the broad and overlapped reflections even when the curve separation technique was applied. Therefore we assumed that the ζ value of a particular layer-line reflection was common to these reflections and determined the unit cell parameters *a* and *b* from the ξ values only. As already reported in a separate paper [19], the ratio of the standard

Table 1
Crystallographic data of the normally-drawn HDPE sample measured at 293 K

Cell parameters	$a = 7.413(20)$ Å, $b = 4.907(15)$ Å, c (fiber axis) $= 2.547$ Å			
Space group	*Pnam*-D_{2h}^{16}			
Fractional coordinates	x/a	y/b	z/c	U_{iso}/Å^2
C	0.4579(13)	0.5621(19)	0.2500	0.069
H	0.3122	0.5244	0.2500	0.106
H	0.4794	0.7829	0.2500	0.106
Anisotropic thermal parameters of carbon atom				
$U_{aa} = 0.084(10)$ Å^2, $U_{bb} = 0.057(9)$ Å^2, $U_{cc} = 0.065(10)$ Å^2,				
$U_{ab} = 0.01(3)$ Å^2				
Intramolecular structural parameters				
C–C = 1.544(9) Å, C–H = 1.095(11) Å, $<$ C–C–C = 111.2(8)°,				
$<$ C–C–H = 109.4(5)°, $<$ H–C–H = 108.1(9)°				
Setting angle of the planar–zigzag chain from the *b* axis = 45.68(30)°				
Total number of observed reflections = 51				
$R_{merge} = 3.0\%$				
Reliability factors $R = 11.59\%$, $R_w = 9.70\%$				

[a] The values shown in parentheses are the standard deviations. For example, $x/a = 0.4579(13)$ is an abbreviated expression of $x/a = 0.4579 \pm 0.0013$

[b] $R_{merge} = \Sigma_i[\Sigma'(I_{io} - \langle I_{io}\rangle)^2/\Sigma I_{io}^2]/N$ where I_{io} is the observed *i*th-intensity and $\langle I_{io}\rangle$ is the average of the intensities between the equivalent four reflections. The summation Σ' is over the equivalent four reflections

$R = 100 \times \Sigma_i(|F_o|_i - |F_c|_i)/\Sigma|F_o|_i$ (%)

$R_w = 100 \times \sqrt{\Sigma w(|F_o| - |F_c|)^2/\Sigma w|F_o|^2}$(%)

Here $|F_o|$ and $|F_c|$ are the observed and calculated structure factors, respectively. $w = \exp[FA \sin^2\theta/(\lambda^2\sigma^2(F_o))]$ where the $\sigma^2(F_o)$ is the squared standard error of the observed structure factor. *FA* was set to 0.0

deviations to the averaged values of the unit cell parameters is in the order of 10^{-3} for most of the normally-analysed crystal structures of the low-molecular-weight compounds. For the present case of PE samples, too, this ratio is in the same order (for example, $\sigma(a)/\langle a\rangle$ is ca. 3/1000 where $\sigma(a)$ and $\langle a\rangle$ are the standard deviation and the averaged value of the *a*-axial length, respectively). The *c*-axial length was determined from the spacings of layer lines, but the thermal contraction was too small to be determined exactly by the present measurements because of short sample-to-camera distance. Therefore the *c* axis was assumed to be constant, 2.547 Å.

As seen in Figs. 5 and 6 the *a* and *b* axes change linearly with temperature but show the deflection points around $+10$°C. The linear thermal expansion coefficients were calculated from the slopes of these linear lines. In Table 2 are compared the linear thermal expansion coefficients of the *a* and *b* axes evaluated for the various PE samples reported so far. Most of these data were obtained for unoriented samples, different from the uniaxially-oriented samples used in the present study. As seen in this table, PE crystal shows the deflection points in the temperature dependencies of the *a* and *b* axes but they are different among the various samples. For example, Swan reported that the linear thermal expansion coefficient α_a was larger as the temperature was increased in the high temperature region (above 50°C) [7]. Schauer and Wilke [16] and Davis et al. [20] showed the existence of deflection points below room temperature but did not report the data above room temperature. These deflection points in the low temperature region are not detected in the present study. The linear expansivity is found to be different between the two types of samples used in the present study. The HDPE sample shows more remarkable temperature dependence of the *a* axis than that observed for the ultradrawn sample. The *b* axis shows also the temperature dependence but the degree of change is not so large as the *a* axis in both the samples.

3.2.2. Crystal structure

The bond length and bond angle of the skeletal chain were calculated from the fractional coordinates and the unit cell parameters. They are found to be almost independent of temperature as shown below.

	bond length	bond angle
	C–C	C–C–C
HDPE	1.543(2) Å	111.4(2)°
ultra-drawn PE	1.540(2) Å	111.7(2)°

Isotropic (U_{iso}) and anisotropic (U_{ij}) atomic displacement parameters, which are proportional to the mean-square displacement $\langle u_{ij}^2\rangle$, are shown in Figs. 7 and 8, respectively, for HDPE and ultra-drawn PE. In the structural analysis, the four types of anisotropic tensor components U_{aa}, U_{bb}, U_{ab}, and U_{cc} were taken into consideration. But U_{ab} is very small compared with the other components (see Table 1) and therefore will not be discussed in detail by taking into consideration the analytical error. The temperature dependencies of the U_{ij} are found to be appreciably different between the ultra-drawn PE and HDPE. U_{aa} and U_{bb} obtained for the HDPE sample show the clear deflection point at about 10°C. The same situation can be seen for the ultradrawn PE sample, although it is a little difficult to see the deflection point. These results are consistent with the result reported by Aoki et al. [9] and Iohara et al. [11]. We may also notice that U_{aa} and U_{bb} of the ultra-drawn PE are very close to each other. The HDPE sample shows a similar tendency in the low temperature region but the thermal parameters increase remarkably in the high temperature region above 10°C. In particular the increase of U_{aa} is more significant than U_{bb}. The displacement parameter along the *c*-axis, U_{cc}, does not show any detectable change around this temperature region.

3.2.3. Setting angle of the planar–zigzag chains

The setting angle is defined as an angle of the zigzag plane of the chain measured from the *b* axial direction. Temperature dependence of the setting angle is shown in Figs 9 and 10, where the temperature factors B_{ii} ($=8\pi^2U_{ii}$) are also plotted against temperature. The setting angle of HDPE is nearly constant below 10°C and increases with increasing temperature above 10°C, confirming the results

Table 2
Linear thermal expansion coefficients of the *a* and *b* axes of PE crystal

Sample	Temperature range	α_a	α_b
ultradrawn PE	180–285 K	$14.0\times10^{-5}\,K^{-1}$	$3.00\times10^{-5}\,K^{-1}$
($\times$ 150 drawn)	285–365	22.2	3.00
HDPE	170–285	21.0	4.35
($\times$ 150 drawn)	285–365	47.8	4.35
HDPE [16]	65–227	13.0	6.20
(unoriented)	227–300	18.0	6.20
HDPE [20]	120–200	13.0	6.10
(unoriented)	230–300	18.5	6.48
HDPE [7]	77–300	15.5	3.85
(unoriented)	300–	increasing gradually	
	411	57.8	−7.3

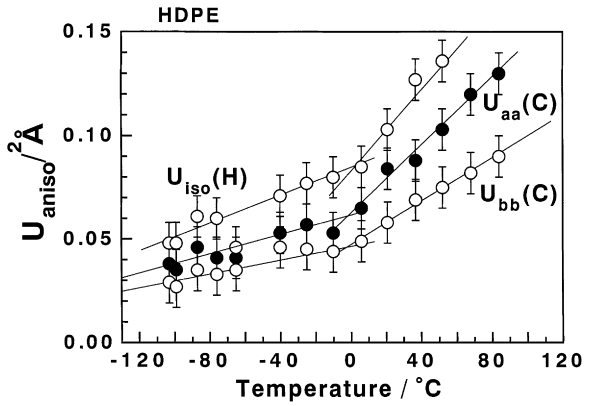

Fig. 7. Temperature dependence of the thermal parameters of carbon (U_{aa} and U_{bb}) and hydrogen (U_{iso}) atoms obtained for orthorhombic crystal of the normally-drawn HDPE sample.

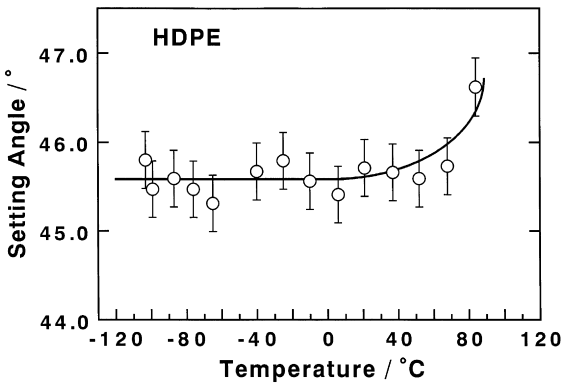

Fig. 9. Temperature dependence of the setting angle of the planar–zigzag chain obtained for orthorhombic crystal of the normally-drawn HDPE sample.

reported by Iohara et al. [11]. Similar tendency is observed also for the ultra-drawn PE sample but the change is very small. The setting angle of HDPE sample is larger than that of the ultra-drawn PE in the whole temperature region.

In this way we found a good correlation between the unit cell dimension a, the displacement parameters U_{aa} and U_{bb}, and the setting angle. The temperature dependence of these structural parameters seems to originate from the anharmonicity of the thermal vibrations in the crystal. The bond length and bond angle were independent of temperature, as stated above, suggesting that the chains may be assumed approximately to be rigid rods in the whole region of temperature investigated here. That is to say, the intramolecular vibrations do not show significant anharmonicity but rather the external vibrations such as translational and/or librational lattice modes are considered to contribute largely to the anharmonic vibration of the crystal, although the skeletal torsional angles might fluctuate more or less with small amplitude around the average value 180° due to the intramolecular thermal vibrations. The thermal parameters U_{ii} or the temperature factors B_{ii} of the carbon atoms are considered also to reflect the anharmonicity of the external vibration. According to the calculation by Kitagawa and Miyazawa [21], the temperature factors are mainly determined by the vibration modes of translational and librational types and are not influenced by the high frequency intramolecular vibrations. As shown in Fig. 11, the thermal parameters calculated by taking into account the anharmonicity under the quasi-harmonic approximation are in good agreement with those analysed here in the temperature region below 10°C. However, the calculated values deviate remarkably above this temperature point. This suggests the quasi-harmonic approximation for the vibrations with infinitesimally small amplitude is broken in the high temperature region. It may be useful to interpret this thermal behavior of PE crystal by carrying out the molecular dynamics calculation.

Iohara et al. [11] and Aoki et al. [9] already pointed out the beginning of anharmonic vibration around 0°C, which has been confirmed in the present paper. It should be noted here that in the present study the uniaxially-oriented PE samples were used. In general the physical property of polymer, even that of the crystalline region is affected sensitively by the morphology change. But the essential

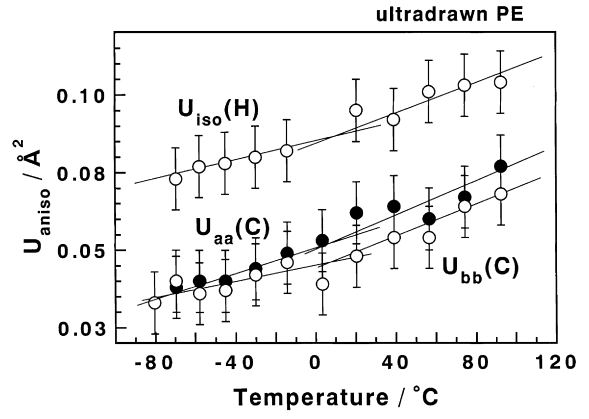

Fig. 8. Temperature dependence of the thermal parameters of carbon (U_{aa} and U_{bb}) and hydrogen (U_{iso}) atoms obtained for orthorhombic crystal of the ultradrawn PE sample.

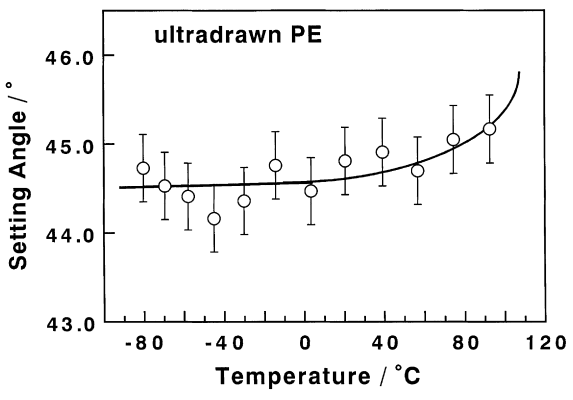

Fig. 10. Temperature dependence of the setting angle of the planar–zigzag chain obtained for orthorhombic crystal of the ultradrawn PE sample.

feature of the thermal behavior of the crystalline part may be said to be almost the same between the unoriented and uniaxially-oriented samples as seen from the comparison of the structural data among the various reports [9,11] and the present study. Besides, we must emphasize here that the data treatment made by us is quantitatively more sophisticated than the studies reported in the previous papers. That is to say, the results obtained in the present study are very important because the structural analysis was made with higher accuracy, originating from the accurate evaluation of the integrated intensities of the reasonably separated reflections and from a much higher number of the observed reflections than those reported so far.

3.2.4. Relationship of deflection point to crystalline dispersion

When the tensile modulus of the uniaxially-drawn PE fiber is measured as a function of temperature, usually several temperature dispersions of the modulus are observed [22]. For example, around -130°C is observed the so-called γ-dispersion, which is said to relate to the local motion of the chain end, branch part, folded chain part, or dislocation in crystalline part [23–25]. The α dispersion is observed to start around 10°C and show the peak at 60–100°C, although these temperatures are dependent on the vibrational frequency used in the dynamic viscoelastic measurement. Dessain et al. reported that the Young's modulus and the tensile strength along the chain axis begin to decrease above 10°C [26]. The temperature 10°C may have a relation with the deflection point revealed by the X-ray structural analysis. We may speculate, for example, that the increase of the inter- and intra-molecular thermal vibrations of zigzag chains cause small but significant change in the chain conformation, which might not be detected by the conventional measurement of the lattice spacing along the chain axis because of too small a change, and affects sensitively the mechanical property of the crystalline part. We have one good example of nylon 6 α crystalline form. The nylon 6 α form was found to show the large temperature dependence of the crystalline Young's modulus along the chain axis [27–29]. The modulus at room temperature is about 165 GPa but it is about 270 GPa at such low temperature as liquid nitrogen temperature [27]. This was ascribed to the small but significant chain contraction due to the thermal vibration of the planar–zigzag chain: only 0.5% contraction of the zigzag chain results in the drastic depression of the Young's modulus from 270 to 165 GPa [27,28]. Although the degree of such thermal motion of planar–zigzag chain might be too small to detect by the X-ray measurement in the present study, we may have one possibility to correlate the beginning of the change in the mechanical property around 10°C with the onset of anharmonic thermal motion of the planar–zigzag chains of PE as likely as in the case of the above-mentioned nylon 6 crystal.

The increment of the thermal vibrations above 10°C may be explained also by another type of relaxation mechanism. For example, the relaxation of the folded chain parts of the lamellar surface causes the rotational motion of the chain stems of the inner parts of the lamellae [24,25]. But the most natural and direct idea to interpret the more enhanced thermal vibration above 10°C seems to be the beginning of the anharmonic lattice vibration of the crystalline lamellae, as discussed above. The true reason why such an anharmonic vibration must be induced in this temperature region should be clarified on the basis of atomistic theory, computer simulation and so on.

3.2.5. Comparison of thermal behavior between the samples

As discussed above, the structural parameters such as the unit cell dimension *a*, thermal parameters, and the setting angle evaluated for the ultra-drawn PE are less temperature-dependent than the case of normally-drawn HDPE sample. We may have two possible ways for the explanation of this difference.

The ultra-drawn PE was prepared by drawing the gel sample by several hundred times the original length. Therefore, the chains are almost fully extended over the whole sample, and the strain on the crystalline region is considered to remain more or less, giving higher restrain on the thermal vibrations of the crystal than the case of normally-drawn HDPE sample. The smaller values of the thermal factors might indicate a reduction of thermal vibrations due to the lattice restraining.

Another interpretation is inverse to the above-mentioned one. The crystalline region of the ultradrawn sample is developed to higher extent than that of the normal HDPE sample, and so is closer to the ideal crystalline state. According to Chatani, Tadokoro et al. [13,14], the setting angle of the PE samples treated under various conditions becomes larger with an increment of the lattice distortion in the *a* (and *b*) direction. From the present analytical result that the setting angle of the ultradrawn sample is smaller than the HDPE sample, it may be considered that the ultradrawn sample shows the smaller lattice distortion because of the well developed crystalline state. The HDPE sample has smaller crystallite size and so the lamellar surface may affect more significantly the various properties of the inner part of the crystallites. The larger temperature dependence of the structural parameters might be related to such an effect of lamellar surface.

For example, Fig. 11 shows the comparison of the thermal parameter U_{aa} between the ultradrawn sample and the normal HDPE sample. According to Kilian [6], the thermal parameters are divided into two parts of the molecular vibrations and the lattice distortion:

$$U = U_{vib} + U_{dist}$$

where U_{vib} and U_{dist} correspond, respectively, to these two terms. U_{dist} can be obtained by extrapolating the temperature dependence curve of the thermal parameters to the absolute zero temperature. Application of this idea to Fig. 11 gives

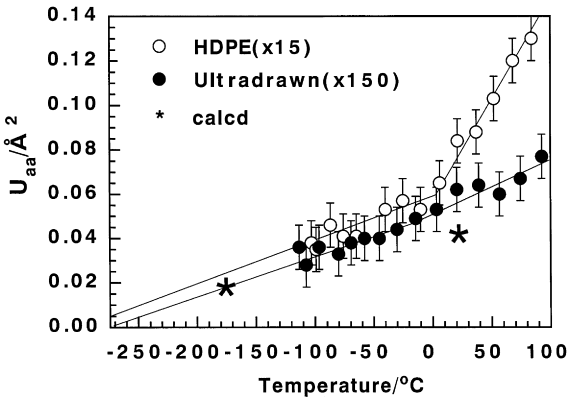

Fig. 11. Comparison of the thermal parameter U_{aa} as a function of temperature between the normally-drawn HDPE and the ultradrawn samples. The extrapolation to absolute zero temperature (− 273°C) gives the thermal parameters originating from the lattice distortion. The points * shown in this figure are the values calculated by Kitagawa and Miyazawa [21].

U_{dist} as follows for the two types of the samples.

$U_{dist} \approx$ 0.000 Å^2 for the ultradrawn sample

$U_{dist} \approx$ 0.003 Å^2 for the normal HDPE sample

U_{dist} is quite small for both the samples, alowing us to assume the thermal parameters obtained in the present analysis come almost purely from the molecular vibrations. Larger U_{dist} value in the normally-drawn HDPE sample suggests higher distorsion of the crystal lattice of this sample than that of the ultradrawn sample. In other words, the ultradrawn PE seems to be more perfect in the crystalline lattice than the normally-drawn HDPE sample.

4. Conclusions

In the present study the temperature dependence of the crystal structure of different types of uniaxially-oriented PE samples was analyzed on the basis of the data collected by the IP system in the temperature region of − 100 to 90°C. This type of structural analysis of PE by using many reflections collected by the IP system may be the first case for the purpose of the investigation of the temperature dependence of the PE crystal structure. Although the experimental error may be still non-negligibly large, we have been able to find quantitatively the several characteristic thermal behaviors of PE crystal. One of these characteristic features is an existence of a deflection point around 10°C. This might be correlated with the beginning of the anharmonic thermal motion of the zigzag chains in the crystal lattice. Besides, these behaviors were found to differ between the normally-drawn and the ultradrawn samples. In order to obtain the true reason of these characteristic features of PE crystal, we need to carry out the theoretical and/or simulation study of the thermal motions of the crystal lattice embedded in the complicated aggregation structure consisting of the crystalline and amorphous regions.

References

[1] Tashiro K. Reports of research project, grant-in-aid for scientific research development of high-quality system for recovering the reliability of X-ray structure analysis of polymer crystals. Japan: The Ministry of Education, Science, Sports and Culture, 1994.
[2] Tashiro K, Nishimura H, Kobayashi M. Macromol Rapid Commun 1996;17:633.
[3] Tashiro K, Asanaga H, Ishino K, Tazaki R, Kobayashi M. J Polym Sci, B: Polym Phys 1997;35:1677.
[4] Miyahara J, Takahashi K, Amemiya Y, Kamiya N, Satow Y. Nucl Inst Meth Phys Res 1986;A246:572.
[5] Bunn CW. Trans Faraday Soc 1939;35:482.
[6] Kilian HG. Kolloid-Z Z Polym 1962;185:13.
[7] Swan PR. J Polym Sci 1962;56:403.
[8] Kasai N, Kakudo M. Rept Progr Polym Phys Jpn 1968;11:145.
[9] Aoki Y, Chiba A, Kaneko M. J Phys Soc Japan 1969;27:1579.
[10] Kavesh S, Schultz JM. J Polym Sci, Part A-2 1970;8:243.
[11] Iohara K, Imada K, Takayanagi M. Polym J 1972;3:357.
[12] Kawaguchi A, Ohara M, Kobayashi K. J Macromol Sci, Phys 1979;B16:193.
[13] Chatani Y, Ueda Y, Tadokoro H. Rep Progr Polym Phys Jpn 1977;20:179.
[14] Tadokoro H. Fiber diffraction methods In: French AD, Gardner KH, editors. ACS Symposium Series vol 141. Washington, DC: American Chemical Society, 1980:43.
[15] Phillips PJ, Tseng HT. Polymer 1985;26:650.
[16] Schauer K, Wilke W. Polymer Bullein 1995;34:477.
[17] Ohta T, Wachi T, Nagai T, Takada A, Ikeda Y, Ohtsubo T, Kawaguchi A. Polymer 1993;34:4863.
[18] Giacovazzo C. Direct methods in crystallography. Academic Press.
[19] Tashiro K, Nishimura H, Kobayashi M. Macromolecules 1996;29:8188.
[20] Davis GT, Eby RK, Colson JP. J Appl Phys 1970;41:4316.
[21] Kitagawa T, Miyazawa T. Abstracts, SPSJ 16th Polymer Symposium, Fukuoka, October 1967:230.
[22] Ohta Y, Yasuda H. J Polym Sci, Part B: Polym Phys 1994;32:2241.
[23] Wada Y, Tusge K. Jpn J Appl Phys 1962;1:64.
[24] Hoffman JD, Williams G, Passaglia E. J Polym Sci 1966;C14:173.
[25] Sinnott KM. J Polym Sci 1966;C14:141.
[26] Dessain et al. J Mater Sci 1992;27:4515.
[27] Miyasaka K, Isomoto T, Koganeya K, Ishikawa K. J Polym Sci, Polym Phys Ed 1980;18:1047.
[28] Tashiro K, Tadokoro H. Macromolecules 1981;14:781.
[29] Nakamae K, Nishino T, Hata T, Matsumoto T. Kobunshi Ronbunshu 1987;44:421.